Received: 15 May 2023 | Revised: 21 November 2023 | Accepted: 23 November 2023

DOI: 10.1111/mmi.15205

RESOURCES

WILEY

Resolving exit strategies of mycobacteria in *Dictyostelium discoideum* by combining high-pressure freezing with 3D-correlative light and electron microscopy

Rico Franzkoch[1,2,3] | Aby Anand[2,4,5,6,7] | Leonhard Breitsprecher[1,2,3] | Olympia E. Psathaki[1,2] | Caroline Barisch[2,4,5,6,7]

[1]iBiOs–integrated Bioimaging Facility, University of Osnabrück, Osnabrück, Germany

[2]Center of Cellular Nanoanalytics, Osnabrück, Germany

[3]Division of Microbiology, Department of Biology, University of Osnabrück, Osnabrück, Germany

[4]Division of Molecular Infection Biology, Department of Biology, University of Osnabrück, Osnabrück, Germany

[5]Centre for Structural Systems Biology, Hamburg, Germany

[6]Division of Host-Microbe Interactome, Research Center Borstel - Leibniz Lung Center (FZB), Borstel, Germany

[7]Department of Biology, University of Hamburg, Hamburg, Germany

Correspondence
Caroline Barisch, Division of Host-Microbe Interactome, Research Center Borstel - Leibniz Lung Center (FZB), Borstel, Germany.
Email: caroline.barisch@cssb-hamburg.de

Olympia E. Psathaki, iBiOs–integrated Bioimaging Facility, University of Osnabrück, Osnabrück, Germany.
Email: katherina.psathaki@uos.de

Funding information
Deutsche Forschungsgemeinschaft, Grant/Award Number: SPP2225(BA6734/2-1,HE1964/24-1), SFB1557-P1 and SFB944-P25

Abstract

The infection course of *Mycobacterium tuberculosis* is highly dynamic and comprises sequential stages that require damaging and crossing of several membranes to enable the translocation of the bacteria into the cytosol or their escape from the host. Many important breakthroughs such as the restriction of mycobacteria by the autophagy pathway and the recruitment of sophisticated host repair machineries to the *Mycobacterium*-containing vacuole have been gained in the *Dictyostelium discoideum*/*M. marinum* system. Despite the availability of well-established light and advanced electron microscopy techniques in this system, a correlative approach integrating both methods with near-native ultrastructural preservation is currently lacking. This is most likely due to the low ability of *D. discoideum* to adhere to surfaces, which results in cell loss even after fixation. To address this problem, we improved the adhesion of cells and developed a straightforward and convenient workflow for 3D-correlative light and electron microscopy. This approach includes high-pressure freezing, which is an excellent technique for preserving membranes. Thus, our method allows to monitor the ultrastructural aspects of vacuole escape which is of central importance for the survival and dissemination of bacterial pathogens.

KEYWORDS
correlative light and electron microscopy, *Dictyostelium discoideum*, freeze substitution, high-pressure freezing, host cell exit, *Mycobacterium marinum*, TEM-tomography, vacuole escape

Rico Franzkoch and Aby Anand contributed equally to this work.

1 | INTRODUCTION

Phagocytosis is a fundamental defence mechanism that triggers inflammatory and immunological responses and plays a crucial role in bridging innate and adaptive immunity against invading pathogens (Lee et al., 2020; Lim et al., 2017). Professional phagocytes such as macrophages and neutrophils use a variety of innate immunity strategies to identify and eliminate intruders within bacteria-containing phagosomes. However, some microbes have developed sophisticated strategies to overcome these processes. For example, *Mycobacterium tuberculosis*, the causative agent of tuberculosis, subverts this compartment into a proliferation-friendly niche while also damaging the membrane and rendering the phagosomal defences ineffective. The host, on the other hand, counteracts by recruiting various membrane repair pathways to the site of damage to retain *M. tuberculosis* inside the *Mycobacterium*-containing vacuole (MCV) (Barisch et al., 2023). When the damage overwhelms the repair machineries, *M. tuberculosis* translocates into the cytosol before exiting the cell (Bussi & Gutierrez, 2019).

We and others have pioneered the investigation of various membrane repair pathways such as ESCRT- and autophagy- (López-Jiménez et al., 2018), as well as ER-dependent repair (Anand et al., 2023) in the *Dictyostelium discoideum*/*M. marinum* model. Within this system, the sequential stages of the *M. tuberculosis* infection course such as (i) the initial stage when the bacteria remodel the phagosome, (ii) the vacuolar stage when replication begins, and (iii) vacuole exit as well as the cytosolic stage that precedes (iv) host cell exit are conserved and are distinguishable with well-established markers (Figure 1) (Cardenal-Munoz et al., 2017). In *D. discoideum*, light microscopy (LM) of live cells has been increasingly important to study the course of infection due to its high temporal and spatial resolution. For example, LM was used to generate time-lapse movies to monitor the escape of *M. marinum* via ejectosomes (Hagedorn et al., 2009), the spatiotemporal dynamics of Rab proteins at the MCV (Barisch, Lopez-Jimenez, & Soldati, 2015) and the re-distribution of lipid droplets during infection (Barisch, Paschke, et al., 2015). Although LM is a powerful tool for observing dynamic processes, it does have limitations. For instance, it relies on selective labelling techniques, e.g., fluorescent proteins or dyes, to visualise subcellular structures or protein localization. Additionally, the relatively low resolution of LM and the absence of ultrastructural context makes it difficult to accurately identify the structures underlying the fluorescence signal. For several decades, transmission electron microscopy (TEM) has been used to unravel the ultrastructural architecture of various organelles. Unlike other techniques, TEM provides near-atomic spatial resolution and allows all subcellular components to be visualised simultaneously (Bozzola & Kuo, 2014). In the *D. discoideum*/*M. marinum* model system, TEM protocols including chemical fixation were used to image ejectosomes (Hagedorn et al., 2009) and to monitor accumulation of intracytosolic lipid inclusions inside *M. marinum* (Barisch & Soldati, 2017). However, conventional sample preparation for EM is known to induce artefacts such as cell shrinkage and extraction of cellular material, which can drastically alter the ultrastructure of the sample (McDonald & Auer, 2006).

The combination of both imaging approaches as correlative light and electron microscopy (CLEM) overcomes the individual limitations and thus represents a robust tool that has recently gained increasing attention in the field of infection biology (Kommnick & Hensel, 2021; Lerner et al., 2020; Weiner et al., 2016). Especially when investigating vacuole escape, reliable preservation and visualisation of the vacuolar membrane is of utmost importance. To overcome the induction of artefacts during sample preparation, high-pressure freezing (HPF) and freeze substitution (FS) were established already in the 1980s (Humbel & Müller, 1985; Moor, 1987). These techniques reduce the occurrence of artefacts and preserve membrane organisation in a near-native state (Kaneko & Walther, 1995; Vanhecke et al., 2008). HPF and FS are therefore essential for analysing the battlefield at the MCV including vacuole damage and escaping pathogens in their ultrastructural environment. However, an approach that combines HPF and FS with CLEM has yet to be established for the *D. discoideum* system. This is very likely due to the fact that *D. discoideum* adhesion points are small, relatively weak and transient (Mijanović & Weber, 2022). Consequently, the ability of *D. discoideum* to adhere to surfaces is relatively low and is very likely the reason for the great loss of cells during HPF and FS. Adherence is critical for CLEM experiments since effective correlation requires the observation of the same cell using both LM and TEM.

The three-dimensional organisation of a cell makes it difficult to detect membrane damage using traditional TEM, as it is limited to capturing two-dimensional sections. High-resolution 3D-EM including TEM-tomography has become an essential tool for accurately identifying membrane discontinuity. For instance, in a recent study,

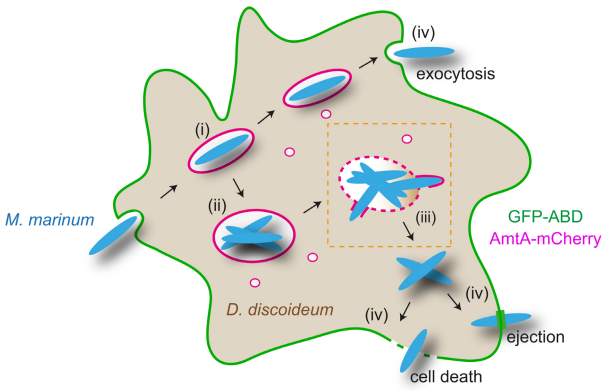

FIGURE 1 Scheme sketching the sequential infection stages of *M. marinum* in *D. discoideum*. Early after uptake, *M. marinum* resides in the MCV (i) and creates a friendly environment for its own replication by blocking phagosome maturation (ii). Cumulative damage at the MCV membrane leads to vacuole escape of the bacteria (iii). *M. marinum* exits *D. discoideum* either by exocytosis, ejection or upon host cell death (iv). The markers GFP-ABD (F-Actin, cell cortex) and AmtA-mCherry (endosomes and MCV) are suited to distinguish various infection stages. The orange box indicates the "infection stage of interest" that was investigated using the here-described workflow.

membrane rupture within mitochondria during apoptosis was elegantly shown using this approach (Ader et al., 2019).

Due to the lack of protocols that allow the visualisation of membrane rupture as well as vacuole escape of *M. marinum*, we developed a 3D-HPF/FS-CLEM workflow for the *D. discoideum*/*M. marinum* system. To this end, we first improved substrate adhesion of *D. discoideum* before combining high resolution fluorescence microscopy, HPF and FS to preserve near-native ultrastructure for TEM-tomography analysis. Our protocol provides a basis for studying exit events in *D. discoideum* and presents the first published 3D-HPF/FS-CLEM protocol for the *D. discoideum*/*M. marinum* model system.

2 | RESULTS

2.1 | Optimising *D. discoideum* adherence and fixation for CLEM

D. discoideum adheres to surfaces via focal-like adhesions that resemble the ones from fibroblasts and other mammalian cells. While these points have been shown to be F-actin positive, *D. discoideum* cell-to-substrate adhesion includes the homologue of talin A and several integrin-like proteins (Cornillon et al., 2008; Kreitmeier et al., 1995; Mijanović & Weber, 2022). However, adhesion points in *D. discoideum* are characterised by their small size (<10% of cell size), fragility, and short lifespan (Weber et al., 1995; Wessels et al., 1994). Tapping the petri dish or pipetting media onto the cells typically results in cell detachment. Therefore, techniques like immunostaining or EM are challenging for adherent *D. discoideum* cells as the standard protocols involve many washing steps. To resolve this issue, we set out to optimise the cell-to-substrate adherence of *D. discoideum*. We took advantage of the fact that the attachment of cells is improved by enhancing their electrostatic interactions by treating surfaces with poly-l-lysine (PLL) (Mazia et al., 1975). Consequently, cell adherence with and without PLL treatment of sapphire discs, i.e., coverslips suitable for HPF was evaluated by LM before and after several washing steps. Without treatment, cells detached from large areas of the discs while PLL coating improved cell adherence (Figures S1 and S2). It should be noted that PLL treatment has been observed to change the morphology of *D. discoideum* and also leads to cell death if exposed for a long time. Thus, we kept incubation times to a minimum of 15 min. However, despite the PLL coating, a high proportion of cells detached after HPF. This was improved when a strain expressing GFP-actin-binding domain (ABD) was used (Figure S2a,b). This strain was originally used to monitor intracellular actin taking advantage of the ABD (Pang et al., 1998). These cells exhibit a high degree of adhesion and are challenging to detach during cell culture. Currently it is poorly understood how the expression of GFP-ABD improves adhesion, however, this might be linked to the fact that foci enriched in F-actin are the anchorage points of traction forces in *D. discoideum* (Iwadate & Yumura, 2008; Mijanović & Weber, 2022). Thus, overexpression of GFP-ABD might increase

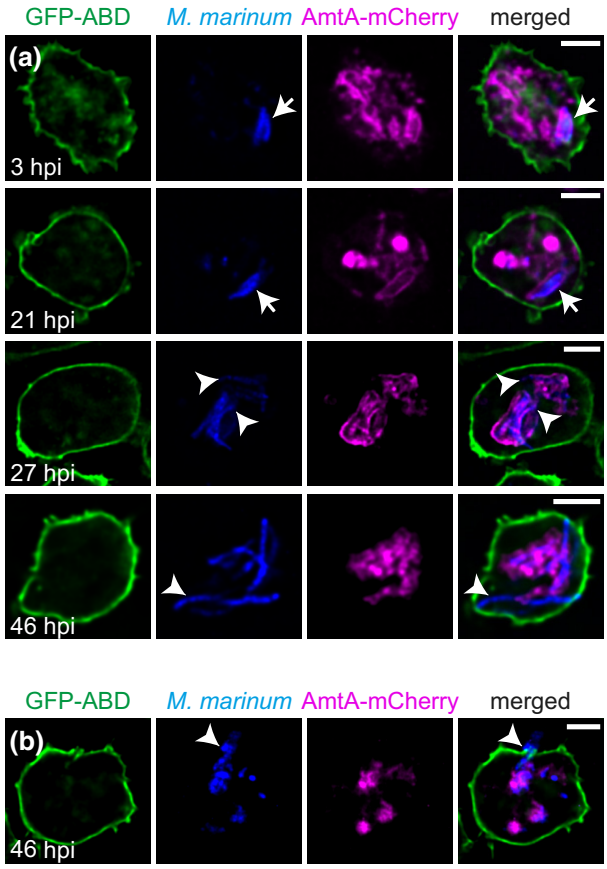

FIGURE 2 The infection course in cells overexpressing AmtA-mCherry and GFP-ABD. *D. discoideum* overexpressing both, GFP-ABD and AmtA-mCherry, were infected with eBFP-expressing *M. marinum*. At the indicated time points, cells were imaged live. Arrows label vacuolar mycobacteria, arrowheads point to either cytosolic mycobacteria in (a) or a bacterium that is exiting the host by ejection in (b). Shown are single planes from z-stacks. Images were deconvolved. Scale bars, 5 μm.

adhesion by cross-linking the F-actin cytoskeleton. To rule out that this leads to artefacts, we performed an infection experiment in cells co-expressing AmtA-mCherry (Figure 2). AmtA is an ammonium transporter that labels all endosomes in *D. discoideum* (Uchikawa et al., 2011) and is a suitable marker for the MCV (Barisch, Paschke, et al., 2015). While GFP-ABD enabled us to monitor MCVs at early infection stages and host cell exit by ejection (GFP-ABD$^+$), AmtA-mCherry allows to visualise MCV membrane rupture and cytosolic bacteria (AmtA-mCherry$^-$) (Figure 2). Importantly, the timing of sequential stages of the infection (Figure 1) appeared to be unaltered by the overexpression of both proteins (Figure 2). In summary, treating sapphires with PLL as well as the overexpression of GFP-ABD significantly improved cell-to-substrate adherence of *D. discoideum* and did not impact the infection course (Figure S2b, Figure 2).

D. discoideum moves a lot and even escapes the imaging field (Barisch, Lopez-Jimenez, & Soldati, 2015). This together with the extremely dynamic nature of its organelles including the MCV, and the time lag between LM and HPF makes the correlation very challenging. To address this, we first tested how different

concentrations of the fixative glutaraldehyde (GA) affect cell shape by seeding *D. discoideum* on sapphire discs and transferring them into an ibidi 8-well dish for live imaging. Next, we carefully added double-concentrated fixative to the cells at final concentrations of 0.05%, 0.1% and 0.5% GA. The recording of the time lapse movies was started 30 sec afterwards. This revealed that low concentrations of GA immobilised the cells, however, their morphology still continued to change (Figure S3a, Movies S1–S4). In addition, we observed cells rounding up especially when incubated with 0.1 and 0.5% GA. We applied a combination of 0.05% GA and 3% paraformaldehyde (PFA), which lead to the subsequent shrinkage of cells (Movie S5). Finally, we discovered that dipping the cells on sapphires into medium containing 2% GA for a short exposure (~1 sec), followed by imaging in 0.5% GA effectively preserved the cell morphology for 30 min (Figure S3a,b, Movie S4). Under these conditions we were able to locate the cells after fixation (Figure S3b) and did not observe any interfering background signals (Figure S3c). A beneficial side effect of the GA fixation was the improved cell adhesion that has already been demonstrated for *D. discoideum* (Koonce et al., 2020).

2.2 | Design of a LM configuration for high numerical aperture oil immersion objectives

Initially, we imaged upright sapphire discs (3*0.05 mm) with cells on top in an ibidi 35 mm dish with a glass bottom or in an 8-well slide with a polymer bottom. In addition, we also tested 35 mm FluoroDishes with glass bottoms. All these vessels have been especially designed by the manufacturers to be combined with high numerical aperture (NA) lenses. Unfortunately, the LM images in all of these combinations were of low quality, most likely because the beam had to pass through two different glass slides, which made it difficult to focus well when using the 40x or inverted 63x oil immersion objectives. We believe that this was caused by (i) the limited working distance of these objectives or by (ii) optical interferences of the bottom of the imaging slide and the sapphire disc.

Subsequently, we designed an imaging setup that is simple to install and used it to acquire LM images of exceptional quality with high NA oil immersion objectives. Figure 3a shows a schematic representation of the entire setup. First, a coordinate system was sputtered onto acid cleaned sapphire discs (3*0.16 mm) using a 20 nm thin layer of gold. Following that, a gold grid with a 2 mm aperture was attached on top of the sapphire disc using Loctite AA 350 to avoid crushing of the cells during the imaging process (Figure 3a, b). This glue has proven to be non-toxic to cells and is non-soluble in water or acetone (Brown, 2012). The assembly was UV-cured overnight in a Leica AFS2 and then coated with PLL. Cells were seeded on top of the sapphire disc with gold spacer at appropriate densities. We used extra thin 24 mm coverslips (130–160 µm) as a bottom for the construct, which was fitted into a custom-made holder onto the microscope stage and sealed with a rubber ring (Figure 3a, c). To prevent cells from drying, 500 µL of HI5c filtered medium containing 0.5% GA were added. The sapphire disc was then flipped upside down and placed on the 24 mm coverslip, resulting in cells directly facing the objective (Figure 3a, c). This enabled high resolution LM imaging using the 63x 1.46 NA oil immersion lens.

2.3 | Workflow of 3D-HPF/FS-CLEM of infected *D. discoideum*

The implementation of our improved cell adhesion and imaging protocols, combined with HPF and FS resulted in highly reproducible outcomes. Briefly, infected cells expressing GFP-ABD

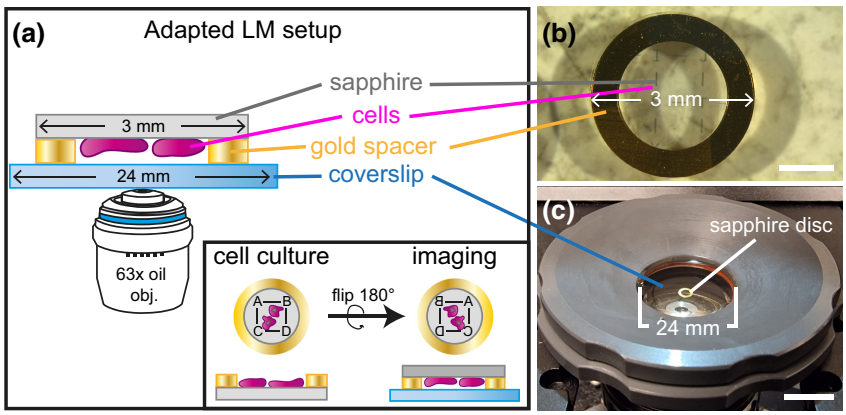

FIGURE 3 Light microscopy imaging setup for optimised z-resolution and correlative work flows. (a) Schematic representation of a 3 mm sapphire disc (grey) with gold spacer (yellow) and monolayer of cells (magenta) on a 24 mm coverslip facing the 63x NA 1.46 oil immersion objective. Rotation of the disc (as indicated in the inset) and application of the gold spacer allows reliable and reproducible focusing since the laser has to pass only through the coverslip. (b) Customization of the sapphire discs. Cells are seeded on sapphire discs with a coordinate system until they form a monolayer of about 70% confluency. (c) Position of the sapphire discs on the stage. The sapphire discs are flipped and placed on a coverslip that is mounted with the help of a custom-made adaptor.

and AmtA-mCherry were seeded on PLL-coated sapphire discs. Prior to LM, the discs were dipped into 2% GA diluted in HI5c filtered medium and transferred upside down with the cells facing the coverslip into the custom-made coverslip holder (Figure 3). Samples were screened for regions of interest (ROI) followed by an acquisition of a z-stack (Figure 4a) and a low resolution brightfield overview (Figure 4b). Following this protocol at least two positions were monitored on each sapphire disc. Directly after acquisition of the last image the sapphires were transferred into the HPF holder with the cells facing upwards (Figure 4c, i). The flat side of a planchette was dipped into 1-hexadecene and added on top of the sapphire. Then the holder was closed and high pressure frozen (Figure 4c, ii). After HPF, the samples were stored in specially designed vessels in liquid nitrogen. These vessels consisted of a 0.5 mL tube with cut-off top and bottom and were used from this point on during the whole FS and embedding procedure. To prevent samples from slipping through the bottom, while also allowing solutions to access the specimen, a fine piece of mesh was attached by slightly melting the end of the tube and pressing it onto the mesh (Figure 4d). This avoids problems that occur when samples are moved to fresh tubes for each step and turned out to be critical in preventing cells from detaching from the sapphires. The protocol for FS is described in Material and Methods. For final polymerisation in EPON 812, sapphire discs with cells facing upwards were transferred into a 0.2 mL PCR tube which was then filled with resin (Figure 4e, i). Polymerised blocks were separated from the tubes with a razor blade. Excess resin on the top and sides of the sapphire was removed. By immersing the top of the block into liquid nitrogen and then touching the sapphire disc with a 50°C warm razor blade, the disc was removed and the EPON surface with cells and coordinate system became visible (Figure 4e, ii). To facilitate trimming and initial correlation, images of the whole block-face were acquired in a scanning EM (SEM) at low vacuum mode (50 Pa) with high probe current (60 A) and voltage (30 kV) (Figure 4f, g). This revealed the gold imprint of the coordinate system on the surface of the EPON block (Figure 4g) and confirmed that the cells remained on the sapphire during the whole procedure thus making a first correlation possible (Figure 4h-j). In addition, this allowed precise targeting and trimming of the block to exclusively include the ROI (Figure 4k). Since *D. discoideum* cells are rather small, it is challenging to precisely identify the cell of interest with a stereomicroscope. Consequently, observation by SEM became incredibly useful. Our SEM system takes less than 30 min to capture SEM data for 6–8 block faces and has no effect on the workflow timetable. Afterwards, semi-thin sections (250 nm) were prepared using an ultramicrotome and deposited on copper slot grids (Figure 4l). With the help of LM and SEM micrographs, the cell of interest was rapidly identified and relocated on the section (Figure 4k). After addition of 10 or 15 nm gold fiducials and contrasting with 3% uranyl acetate for 30 min and 2% lead citrate for 20 min correlative TEM tomograms with a tilt range from ±60° were acquired (Figure 4l).

2.4 | 3D-HPF/FS-CLEM to monitor the ultrastructure of vacuolar escape of *M. marinum* in *D. discoideum*

To showcase the applicability of our developed 3D-HPF/FS-CLEM workflow, we set out to resolve and correlate the ultrastructure of the MCV during vacuolar escape of *M. marinum* in *D. discoideum*. Cells co-expressing GFP-ABD and AmtA-mCherry were infected with eBFP-expressing bacteria and analysed at 24 hours post-infection (hpi) (Figure 5a). During LM we partly observed absence of the AmtA-mCherry signal on the MCV indicating that there might be membrane rupture at the site of escape (Figure 5b, arrowheads). However, without the underlying ultrastructural information, this interpretation remains speculative. The previously described 3D-HPF/FS-CLEM workflow enables precise correlation of areas without AmtA-mCherry signal with high resolution tomography data (Figure 5b, Movies S6 and S7). This revealed one single MCV containing at the same time a large membrane rupture with partially cytosolic bacteria (Figure 5c), as well as a small membrane lesion in close proximity to vacuolar bacteria (Figure 5d). Additionally, we correlatively investigated the subcellular environment of RD1-deficient (ΔRD1) *M. marinum* during infection of *D. discoideum* (Figure 6). This mutant lacks the "region of difference 1" locus and fails to cause membrane damage and rarely escapes into the cytosol (Barisch, Paschke, et al., 2015; López-Jiménez et al., 2018). Consistent with this, the bacteria are residing within intact MCVs (Figure 6a-c, Movie S8) which underlines the excellent preservation of membranes and the reproducibility of the workflow presented here.

To highlight the improved ultrastructural preservation of HPF/FS over conventional (CE) sample preparation, we conducted a side-by-side comparison of both procedures (Figure S4). This revealed that in specimen prepared with HPF/FS, the cytosol is consistently densely packed with cytoplasmic content while numerous vacant spaces were observed when CE sample preparation was used (Figure S4a,b). In addition, the lipid bilayer of various cell organelles exhibits remarkable clarity after HPF/FS and cytosolic mycobacteria appear to be closely surrounded by cytoplasmic material (Figure S4c–e). In contrast, following CE, notable gaps often appeared between the bacteria and the surrounding cytosol, presumably resulting from shrinkage (Figure S4f).

In conclusion, our approach enables the efficient correlation of LM and EM data, and facilitates an accurate and comprehensive understanding of subcellular structures and dynamic processes such as vacuole escape with nearly native ultrastructural preservation.

3 | DISCUSSION

In this article, we describe a robust 3D-HPF/FS-CLEM workflow that integrates LM, HPF, FS and TEM-tomography for studying exit events in the *D. discoideum*/*M. marinum* model system. To this end, we created a unique LM setup which facilitates high resolution LM using high numerical aperture oil immersion lenses that is also compatible with live

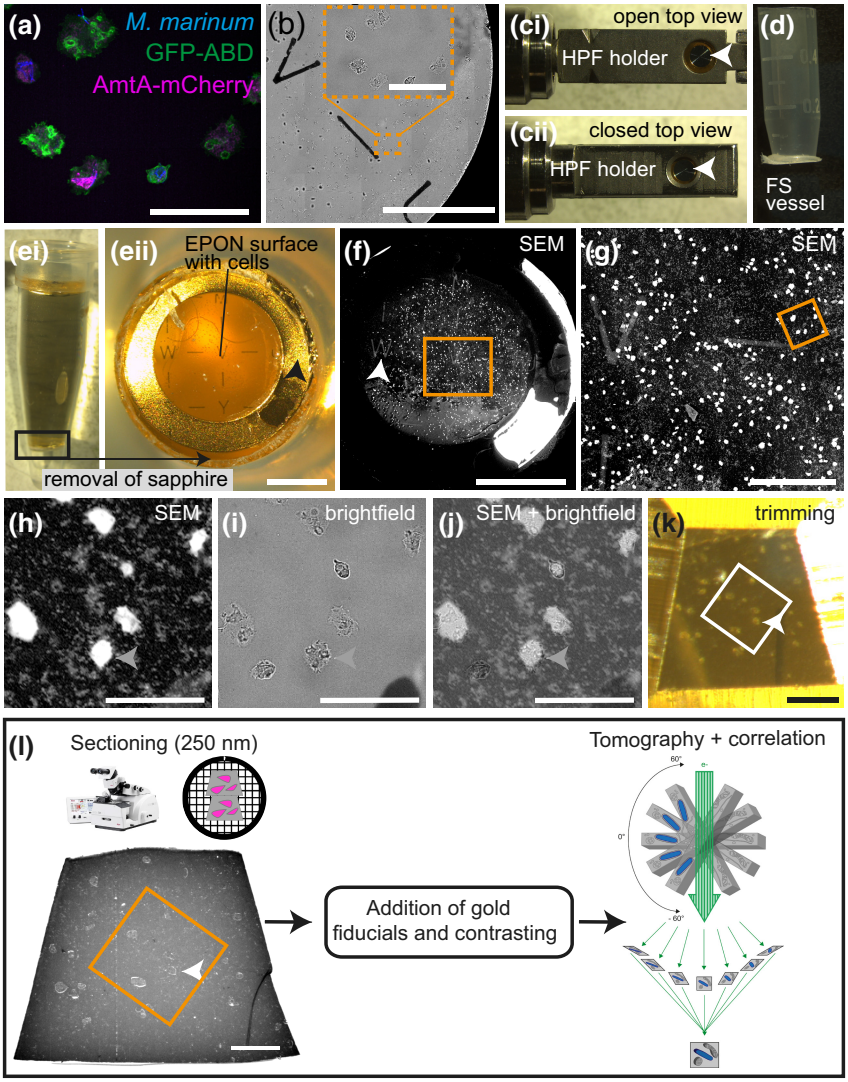

FIGURE 4 3D-HPF/FS-CLEM workflow. (a) Locating the cell of interest and fluorescence z-stack acquisition of fixed cells by SD microscopy using the 63x objective. (b) An overview is acquired using either the 25x oil immersion or 10x air objective to visualise the coordinates of the desired region (orange box). (c) Assembly of the sandwich consisting of a flat planchette dipped in 1-hexadecene and the sapphire with gold spacer and cells is assembled in the HPF-holder (i). With the redesigned carrier, the holder can be closed properly and HPF can be initiated (ii). (d) After HPF, sapphire discs are placed in a special vessel that facilitates storage in liquid nitrogen and their further processing. (e) Embedding of cells in a 0.2 mL tube that is filled with EPON 812 (i) and removal of the sapphire via heat shock which leaves the resin with cells, the gold spacer and the coordinates on top (ii, black arrowhead). (eii) Bottoms-up view of (ei). (f–j) Locating the cells of interest (orange arrowheads) by acquiring an overview using SEM in which the gold coordinates are easily visible (f, white arrowhead), zoom of orange box in f (g), zoom of orange box in g (h), bright field image of the SEM region shown in h (i) and its overlay (j). (k) Trimming of the ROI and sectioning of 250 nm semithin sections using an ultramicrotome facilitated by the previously recorded LM and SEM images. Sections are then transferred onto copper grids. (l) Addition of gold fiducials and contrasting agents prior to tomogram acquisition and correlation. Arrowheads in (eii), (f), (h) - (l) indicate the cell of interest. White or orange boxes in (k) and (l) indicate the ROI. Image in (a) was deconvolved. Scale bar, 50 µm in (a), (h), (i), (j); 500 µm in (b); 1 mm in (e; i, ii); 200 µm in (g) and (l); 100 µm in (k).

cell imaging (Figure 3, Movies S1–S5). However, because of the time delay of up to 1 min between acquisition of the last LM image and HPF, we decided to include a mild fixation step. This immobilises *D. discoideum* and allows precise correlation of LM and TEM-tomography. A system that allows even faster transfer of the sample to the HPF machine, was developed by Verkade in 2008. To this end, LM and HPF are carried out in the same holder (Verkade, 2008). Using this setup, time until cryo-fixation was reduced to up to four seconds (Brown, 2012). This configuration is only available from Leica which severely limits its use. Another comparable setup was recently presented by Heiligenstein et al. (2021) consisting of the HPM live µ high-pressure freezer in combination with the CryoCapsule. Here, the process from LM to cryo-fixation is completely automated and happens within 1.2 seconds. The recent advancements in holder and transfer systems underline the urgent need for new methodological approaches for sample carriers and preparation for CLEM including HPF. In this regard, we established a method which does not require further equipment and allows precise correlation of ROIs monitored by LM (Figures 3 and 4). Nevertheless,

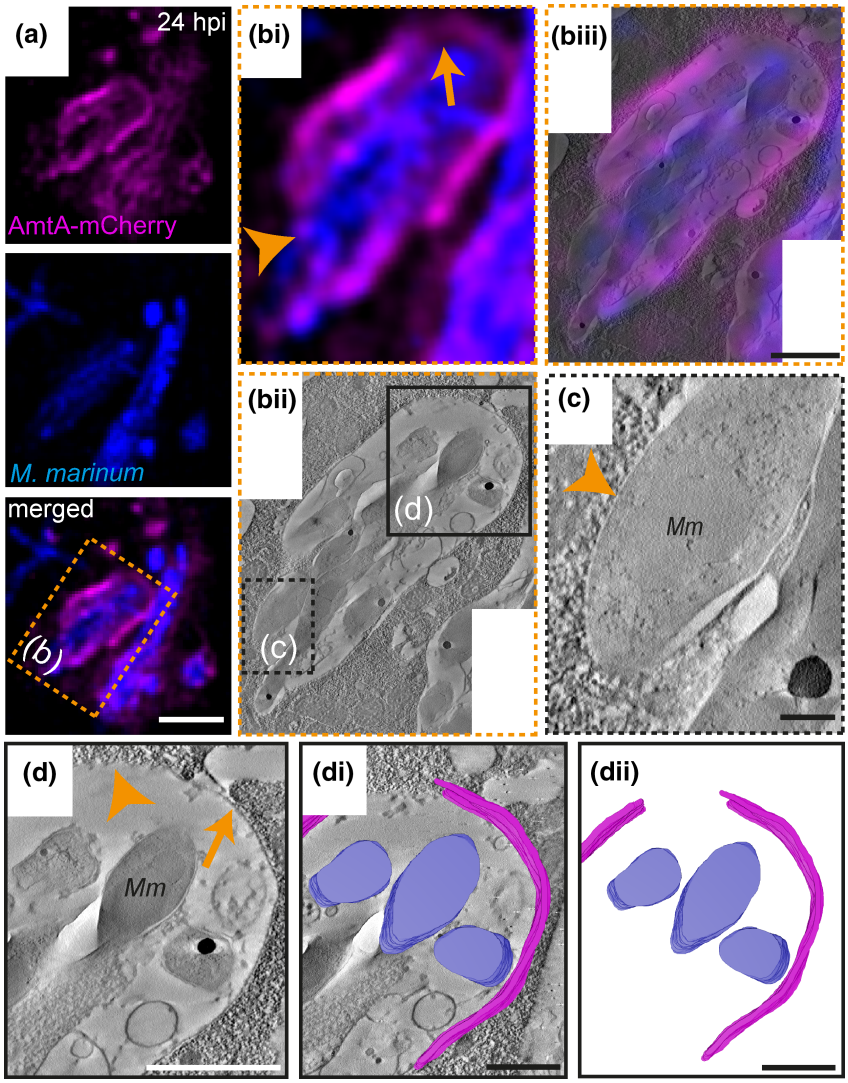

FIGURE 5 3D-HPF/FS-CLEM enables the visualisation of *M. marinum* exiting the MCV. (a) Fluorescence image showing the vacuolar translocation of *M. marinum*. (b) Correlation of the magnified LM image with the tomogram; (i) LM image showing membrane ruptures reflected by the loss of the AmtA-mCherry signal (arrow: minor lesion, arrowhead: full rupture). (ii) Corresponding tomography slice. (iii) Overlay of both imaging modalities to identify possible exit events. (c-d) Higher magnification tomograms of the areas indicated in (bii) revealed a bacterium that is fully cytosolic (c, arrowhead) and bacteria that are partially enclosed by the membrane of the MCV (arrow). (d) The gap in the MCV membrane correlates with the absence of the AmtA-mCherry signal (arrowhead). (di, dii) This is supported by the segmentation showing a discontinuity of the MCV membrane throughout the whole tomogram. Blue: *M. marinum*, magenta: MCV membrane. *Mm*: *M. marinum*. Image in (a) was deconvolved. Scale bar, 5 μm (a), 1 μm (b), 200 nm (c), 1 μm (d). Please see also Movies S6 and S7.

there is a need for the development of systems that enable swift transfer between LM and HPF. Additional modifications of our method would include the design of an LM setup in which LM is directly carried out through the bottom of the sapphire disc rather than through the coverslip. In this arrangement cells would be closer to the objective lens resulting in high-quality fluorescence images, however, construction and handling of such a system would be more challenging.

Key advantages of utilising HPF and FS are near-native preservation of ultrastructure including membranes, which present important barriers pathogens have to overcome (Kaneko & Walther, 1995; McDonald & Auer, 2006; Vanhecke et al., 2008). For the *D. discoideum/M. marinum* model system only few CLEM approaches are published (Gerstenmaier et al., 2015; Malinovska et al., 2015). They all include conventional sample preparation for EM, which may not accurately reflect the native membrane organisation in the investigated specimens and complicates data interpretation. A general challenge for setting up CLEM with *D. discoideum* is the fact that these cells adhere only weakly to the substrate (Weber et al., 1995; Wessels et al., 1994). To overcome this, we used a strain expressing GPF-ABD, which enhances cell-substrate adhesion, combined with PLL coating of sapphire discs and mild GA fixation, which dramatically improved the success of the protocol (Figures S1–S3). Coating substrates with PLL is a well-known method to improve adherence in cell culture and also provided excellent results for *D. discoideum* (Lombardi et al., 2008). Fixation with low concentrations of GA has been previously shown to promote cell attachment in *D. discoideum* and was suggested to be used when several washing or incubation steps are involved (Koonce et al., 2020). Even when chemical fixation is employed prior to HPF, ultrastructural preservation is drastically enhanced (Figures 5 and 6, Figure S4), indicating that the most problematic steps in the conventional sample preparation protocol are indeed post-fixation and especially dehydration (Small, 1981). This procedure is applicable for a wide range of specimens ranging from highly labile tissues to cells infected with Hepatitis C virus (Romero-Brey & Bartenschlager, 2015; Sosinsky et al., 2008).

Since TEM-tomography achieves high resolution 3D-data for volumes below 500 nm semi-thin sections, a great improvement to understand escape of pathogens would be to also visualise whole cells or larger volumes. For conventional sample preparation this has been already shown for *M. marinum* infected *D. discoideum* and other host-pathogen systems such as epithelial cells infected with *Shigella*

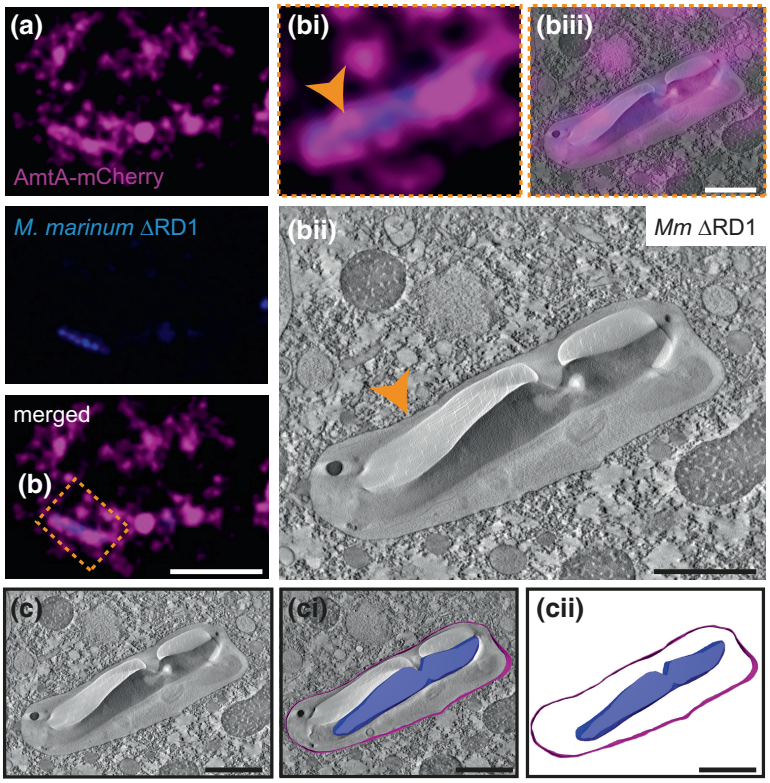

FIGURE 6 3D-HPF/FS-CLEM enables the visualisation of *M. marinum* ΔRD1 inside intact MCVs. (a) Fluorescence images showing the bacteria inside an AmtA-mCherry$^+$ vacuole. (b) Correlation of the magnified LM image with the tomogram; (i) LM image showing an intact MCV reflected by completeness of the AmtA-mCherry signal (arrowhead: intact membrane). (ii) Corresponding tomogram slice. (iii) Overlay of both imaging modalities to highlight the continuity of the membrane. (c) This is further illustrated by segmentation and model generation (ci, cii). Blue: *M. marinum*, magenta: MCV membrane. Image in (a) was deconvolved. Scale bar, 10 μm (a), 1 μm (b, c). Please also see Movie S8.

(Anand et al., 2023; López-Jiménez et al., 2018; Weiner et al., 2016). In principle, specimens prepared using the here-developed workflow could be directly processed through techniques such as focused ion beam (FIB)-SEM or similar methods, which offer high volumetric information with EM resolution (Collinson et al., 2023; Villinger et al., 2012). This further underscores the versatility of our approach and will enable correlation in three dimensions, allowing the reconstruction of entire organelles beyond the limitations of semi-thin sectioned volumes. The use of coordinate imprints is sufficient for correlating cell monolayers and eliminates the need for additional artificial landmarks to guide EM acquisition after embedding (Ronchi et al., 2021). By employing these techniques, correlation precision (Krentzel et al., 2023), throughput (Serra Lleti et al., 2022) and extended downstream analysis of host-pathogen interactions at contact sites of organelles and pathogenic compartments could be improved (Anand et al., 2023; Weiner & Enninga, 2019). Similar techniques have been used to reveal new insights into the replicative niche of *Mycobacterium tuberculosis* (i.e., fluorescence imaging of live or fixed cells combined with conventional SBF-SEM (Russell et al., 2017)) or the interaction of autophagosomes with *M. tuberculosis* (i.e., post-fixation confocal imaging combined with conventional sample preparation for FIB-SEM (Bernard et al., 2020)). However, our methodology differs from existing methods in the context of containing only a brief exposure to GA and especially the integration of HPF/FS to improve the overall ultrastructural quality and correlation efficacy.

An alternative to be independent of cell adherence is to perform LM directly on the embedded sample (Ader & Kukulski, 2017; Kukulski et al., 2011). However, this restricts the examination to those cells that remain within the resin block after embedding. Given that sectioning typically covers relatively small areas (~0.12 μm^2) the number of cells drastically decreases when compared to the comprehensive screening of a whole sapphire disc (~7 μm^2). This would make detection of rare events even more challenging. Recently, a very intriguing approach that circumvents this issue was developed (Ronchi et al., 2021). Here the whole block was analysed by LM enabling the screening of the complete sapphire disc and precise targeting of cells of interest for subsequent trimming, sectioning, or even FIB-SEM acquisition. These strategies represent promising avenues for visualising interactions between *D. discoideum* and *M. marinum* in the future.

Overall, our workflow provides the first approach to correlatively visualise adherent *D. discoideum* cells infected with *M. marinum* in a more native state using HPF and FS. This allows data to be evaluated more accurately and vacuole escape to be detected with near-atomic spatial resolution in three dimensions. The low cost and ease of implementation of our approach also have important advantages for monitoring membrane damage and exit events in other infection systems.

4 | EXPERIMENTAL PROCEDURES

4.1 | *D. discoideum* strains and cell culture

All the *D. discoideum* material is listed in Table S1. *D. discoideum* wild type (AX2) was cultured axenically at 22°C in HI5c medium (Foremedium) in the presence of 100 U/mL penicillin and 100 μg/

mL streptomycin, respectively. The GFP-ABD expressing cells were electroporated with pDM1044-AmtA-mCherry (Barisch, Paschke, et al., 2015) and grown in HI5c containing the respective antibiotics (hygromycin 50 μg/mL and G418 at 5 μg/mL).

4.2 | Mycobacteria strains and cell culture

All the *M. marinum* material is listed in Table S1. *M. marinum* was cultured in 7H9 medium supplemented with 10% OADC, 0.2% glycerol and 0.05% Tween-80 at 32°C in shaking at 150 rpm until an OD_{600} of 1 (~1.5×10^8 bacteria/mL). To prevent bacteria from clumping, flasks containing 5 mm glass beads were used. To generate wt or ΔRD1 mycobacteria expressing eBFP, the unlabelled strains were transformed with the pTEC18 plasmid and cultured in medium containing 25 μg/mL hygromycin.

4.3 | *D. discoideum* infection with *M. marinum*

To prepare *D. discoideum* for infection, cells were grown overnight in 10-cm dishes in media devoid of antibiotics until confluency. The infection was carried out as previously described (Barisch, Lopez-Jimenez, & Soldati, 2015; Hagedorn & Soldati, 2007). Briefly, for a final multiplicity of infection (MOI) of 10 (wt) or of 20 (ΔRD1), 5×10^8 (wt) or 1×10^9 (ΔRD1) bacteria were washed twice and resuspended in 500 μL HI5c. To remove clumps, bacteria were passed 10 times through a 25-gauge needle and added to a 10-cm dish of *D. discoideum* cells. To increase the phagocytosis efficiency, the plates were centrifuged at 500 g for two times for 10 min at RT. After 20–30 min, the extracellular bacteria were removed by several washes with HI5c filtered medium. Finally, the infected cells were taken up in 30 mL of HI5c (filtered) at a density of 1×10^6 cells/mL supplemented with 5 μg/mL streptomycin and 5 U/mL penicillin to prevent growth of extracellular bacteria and incubated at 25°C at 130 rpm. At 24 hpi, samples were taken and prepared for live imaging.

4.4 | Preparation of sapphire discs

Before usage, sapphire discs (3 mm × 0.16 mm) were acid cleaned. To this end, the discs were soaked in 3.7% hydrochloric acid (HCl) for an hour on a tumbler, washed with de-ionised water, with 100% ethanol and air dried. Next, sapphires were equipped with a coordinate system by gold sputtering and a gold spacer to optimise image acquisition. The spacer consisted of a 3 mm gold grid (G2620A, Plano) with a central aperture of 2 mm and was glued onto the sapphire disc using Loctite AA 350 (Henkel, Hemel Hempstead, UK). The glue was polymerised overnight in a Leica AFS2. To improve cell adherence, sapphires were then incubated with 1 mg/mL PLL (P1274, Sigma) for 3 h at 37°C. Unbound PLL was removed by three washes with double distilled water, air dried on Kimtech paper (#7552, Diagonal) and stored at RT.

4.5 | Pre-fixation and fluorescence imaging by spinning disc confocal microscopy

6–8 PLL-coated sapphire discs were washed twice with HI5c (without antibiotics) and placed in a 2-well μ-ibidi. Prior to the experiment, the sapphire discs were checked under a light microscope for handling errors. 70% confluent sapphires were prepared by adding the cells and frequent inspection with a cell culture microscope. To remove floating cells, the medium was then replaced with fresh HI5c filtered medium. For the adherence test (-PLL vs. +PLL, AmtA-mCherry vs. AmtA-mCherry/GFP-ABD), cells were seeded on 10 mm coverslips. Images were captured before and after a gentle washing procedure. To this end, the coverslips were grasped with tweezers and briefly immersed 6–8 times in the cell culture medium. Cells were counted manually, plots and statistical tests were generated using GraphPad Prism.

For the fixation test, the sapphires with cells were briefly dipped into 2% GA in HI5c filtered and transferred with the cells and gold spacer facing the objective into a custom holder containing 0.5% GA in HI5c filtered for light microscopy prior to image acquisition. The bottom of the holder consisted of an extra thin 24 mm round coverslip with a nominal thickness of 130–160 μm (KHX8.1, Roth). Other vessels that were unsuccessfully tested included an ibidi 35 mm μ-dish with a glass bottom (81,158, ibidi), an ibidi 8-well μ-slide (80,806, ibidi) and a 35 mm Fluorodish (FD35-100, WPI).

The Zeiss Cell Observer.Z1 is an inverted microscope, fully motorised and equipped with a Yokogawa Spinning Disc Unit CSU-X1a 5000 with a custom-built acrylic glass incubation chamber. The chamber was set to 25°C, 30 min prior to image acquisition. Alpha Plan-Apochromat 63x (NA 1.46, TIRF, oil immersion equipped with DIC slider EC PN 63x 1.25 III, CA 63x/1.2 W III), Plan-Apochromat 40x (NA 1.4, DIC, oil immersion equipped with DIC slider CA 40x/1.2 W, LD CA 40x /1.1 W III), LD LCI Plan-Apochromat 25x (NA 0.8, DIC, immersion: oil, water, and glycerin, equipped with DIC slider LCI PN 25x/0.8 II) and Plan-Neofluar 10x (NA. 0.3, DIC I, Ph 1, air) were used as objectives. The system is equipped with computer-controlled multi-colour laser module with AOTF combiner (405 nm diode laser, max. power 50 mW, 488 nm optically pumped semiconductor laser, max. power 100 mW, 561 nm diode laser, max. power 40 mW, 635 nm diode laser, max. power 30 mW). The photometrics Evolve EMCCD camera was used and contained filters for blue (Zeiss Filter set 49), eGFP (Zeiss Filter set 38 HE) and Cy3 (Zeiss Filter set 43 HE). An area of 512 × 512 pixels with binning 1 × 1 was imaged with laser power of 20% to 30% for 488 nm, 10% to 20% for 405 nm and 40% to 50% for 561 nm. All channels were captured with a 100 ms exposure time. For all channels a Z-stack with a spacing of 220 nm was acquired for 19 (wt) or 40 (ΔRD1) optical slices and a total volume of 4180 or 8800 nm, respectively. Data was acquired

in Zeiss ZEN 2012 (blue edition) and stored in the OMERO 5.6.4 database. Images were processed using FIJI/ImageJ (version 1.54f) and deconvolved with the Huygens Remote Manager (version v3.7.1) from Scientific Volume Imaging (Netherlands) using the classic maximum likelihood estimation algorithm with 40 iterations and 0.01 quality change.

4.6 | High pressure freezing (HPF)

Directly after acquisition of the last light microscopy image, sapphire discs were further processed for HPF. To this end, the discs were placed with the cells and gold spacer facing the flat side of a 3 mm aluminium planchette no. 242 (Engineering Office M. Wohlwend GmbH, Sennwald, Switzerland) which was dipped into 1-hexadecene (822,064, Merck). Subsequently, the assembly was placed in the HPF-holder and immediately frozen using a Wohlwend HPF Compact 03 high-pressure freezer (Engineering Office M. Wohlwend GmbH, Sennwald, Switzerland). The vitrified samples were stored in homemade storage vessels consisting of 0.5 mL tubes with cut-off tops and bottoms. A fine mesh was bonded to the bottom to allow the flow of solutions to the samples while preventing them from falling.

4.7 | Freeze substitution (FS)

Prior to FS, the aluminium planchettes were separated from the sapphire discs in liquid nitrogen. All steps were conducted with sapphire discs in aforementioned vessels. The sapphire discs were then immersed in a substitution solution containing 1% osmium tetroxide (19,134, Electron Microscopy Sciences), 0.1% uranyl acetate (E22400, Electron Microscopy Sciences) and 5% H_2O in anhydrous acetone (83683.230, VWR) pre-cooled to −90°C. The FS was performed in a Leica AFS2 (Leica, Wetzlar, Germany): 27 h at −90°C, 12 h at −60°C, 12 h at −30°C and 1 h at 0°C. After 5 washes with anhydrous acetone on ice, the discs were stepwise embedded in EPON 812 (Roth, Karlsruhe, Germany), incubated with acetone (30% EPON, 60% EPON, 100% EPON) and finally polymerised for 48 h at 60°C. After removal of the sapphire disc utilising liquid nitrogen and a hot razor blade, semithin sections of 250 nm were cut with a Leica UC7 ultramicrotome using diamond knives (Diatome, Switzerland). Sections were collected on formvar-coated grids and post-stained for 30 min with 2% uranyl acetate and 20 min in 3% lead citrate and analysed with a JEM 2100-Plus (Jeol, Japan) operating at 200 kV equipped with a 20-megapixel CMOS XAROSA camera (EMSIS, Muenster, Germany).

4.8 | Tomography acquisition

For TEM-tomography, 250 nm thick sections were labelled with 10 or 15 nm protein-A-gold fiducials on both sides prior to post-contrasting. Tilt series were acquired from ±60° with 1 ° increments using the TEMography software (Jeol, Japan) and a JEM 2100-Plus operating at 200 kV and equipped with a 20-megapixel CMOS XAROSA camera (EMSIS, Muenster, Germany). Nominal magnifications and pixel size were 10,000× and 0.94 nm (Figure 5b-e) and 15,000× and 0.62 nm (Figure 5f).Tomograms were reconstructed using the back projection algorithm in IMOD (Kremer et al., 1996). Segmentation was done manually using IMOD or Microscopy Image Browser (Belevich et al., 2016) (version 2.84) and animations were visualised using Amira-Avizo (Thermo Fisher Scientific, Waltham, USA) (version 2022.1). For visualisation of the MCV in Figure 5b-d two independent tomograms were stitched together using Amira-Avizo.

4.9 | Conventional EM sample preparation

For conventional sample preparation (Barisch, Paschke, et al., 2015), infected *D. discoideum* was fixed with 2% GA in HI5c for 1 h at RT and subsequently overnight at 4°C. Samples were washed with 0.1 M imidazole buffer (pH 7.5) and post-fixed with 2% osmium tetroxide in 0.1 M imidazole buffer for 1 h at RT in the dark. Specimens were rinsed five times with H_2O and incubated for 1 h in 1% uranyl acetate at RT in the dark. After three washing steps with H_2O, cells were dehydrated in a series of anhydrous ethanol (10 min in 30%, 50%, 70%, 80%, 90%, 100%, 100%) and 100% anhydrous acetone (2× 10 min). Infiltration with EPON 812, polymerisation, ultramicrotomy and post-contrasting was carried out as described above (see section "*Freeze substitution*").

4.10 | Scanning electron microscopy

Following the removal of the sapphire discs, EPON blocks were placed onto adhesive conductive carbon tabs positioned on a metal sheet, ensuring the cell side of the block faced upwards. Subsequently, the samples were introduced into a Jeol JSM-IT200 (Jeol, Japan) and images were recorded using the BED-C detector at a low vacuum of 50 Pa, an accelerating voltage of 30 kV and a probe current of 60.

AUTHOR CONTRIBUTIONS

Caroline Barisch: Conceptualization; funding acquisition; writing – original draft; validation; writing – review and editing; project administration; supervision; resources. **Rico Franzkoch:** Conceptualization; investigation; writing – original draft; writing – review and editing; visualization; formal analysis; software; data curation; methodology; validation. **Aby Anand:** Conceptualization; investigation; writing – original draft; visualization; writing – review and editing; software; formal analysis; data curation; methodology; validation. **Leonhard Breitsprecher:** Data curation; software; visualization; writing – review and editing. **Olympia E. Psathaki:** Conceptualization; funding acquisition; validation; writing – review and editing; project administration; supervision; resources.

ACKNOWLEDGMENTS

We greatly acknowledge the light microscopy unit of the integrated Bioimaging facility (iBiOs) at the University of Osnabrück and especially Rainer Kurre and Michael Holtmannspötter for their expertise and friendly support. This project was supported by the DFG: SPP2225 (CB: BA 6734/2-1), SFB944 (CB: P25) and SFB1557 (CB: P1). We especially thank Michael Hensel for supporting this work via the iBiOs imaging platform that is part of the SPP2225 (MH: HE 1964/24-1). Open Access funding enabled and organized by Projekt DEAL.

CONFLICT OF INTEREST STATEMENT

The authors declare that they have no conflict of interest.

DATA AVAILABILITY STATEMENT

The data that support the findings of this study are available from the corresponding author upon reasonable request.

ETHICS STATEMENT

No human or animal subjects or materials were used in this article.

ORCID

Caroline Barisch https://orcid.org/0000-0002-1493-9006

REFERENCES

Ader, N.R., Hoffmann, P.C., Ganeva, I., Borgeaud, A.C., Wang, C., Youle, R.J. et al. (2019) Molecular and topological reorganizations in mitochondrial architecture interplay during Bax-mediated steps of apoptosis. *eLife*, 8, e40712.

Ader, N.R. & Kukulski, W. (2017) triCLEM: combining high-precision, room temperature CLEM with cryo-fluorescence microscopy to identify very rare events. In: Müller-Reichert, T. & Verkade, P. (Eds.) *Methods in cell biology*. Cambridge, MA: Academic Press.

Anand, A., Mazur, A.C., Rosell-Arevalo, P., Franzkoch, R., Breitsprecher, L., Listian, S.A. et al. (2023) ER-dependent membrane repair of mycobacteria-induced vacuole damage. *mBio*, 14, e0094323.

Barisch, C., Holthuis, J.C.M. & Cosentino, K. (2023) Membrane damage and repair: a thin line between life and death. *Biological Chemistry*, 404, 467–490.

Barisch, C., Lopez-Jimenez, A.T. & Soldati, T. (2015) Live imaging of Mycobacterium marinum infection in *Dictyostelium discoideum*. *Methods in Molecular Biology*, 1285, 369–385.

Barisch, C., Paschke, P., Hagedorn, M., Maniak, M. & Soldati, T. (2015) Lipid droplet dynamics at early stages of Mycobacterium marinum infection in Dictyostelium. *Cellular Microbiology*, 17, 1332–1349.

Barisch, C. & Soldati, T. (2017) Mycobacterium marinum degrades both triacylglycerols and phospholipids from its Dictyostelium host to synthesise its own triacylglycerols and generate lipid inclusions. *PLoS Pathogens*, 13, e1006095.

Belevich, I., Joensuu, M., Kumar, D., Vihinen, H. & Jokitalo, E. (2016) Microscopy image browser: a platform for segmentation and analysis of multidimensional datasets. *PLoS Biology*, 14, e1002340.

Bernard, E.M., Fearns, A., Bussi, C., Santucci, P., Peddie, C.J., Lai, R.J. et al. (2020) M. Tuberculosis infection of human iPSC-derived macrophages reveals complex membrane dynamics during xenophagy evasion. *Journal of Cell Science*, 134, jcs252973.

Bozzola, J. & Kuo, J. (2014) *Electron microscopy: methods and protocols*. New York: Humana Press.

Brown, E., Van Weering, J., Sharp, T., Mantell, J. & Verkade, P. (2012) Capturing endocytic segregation events with HPF-CLEM. In: Müller-Reichert, T. & Verkade, P. (Eds.) *Methods in cell biology*. Cambridge, MA: Academic Press.

Bussi, C. & Gutierrez, M.G. (2019) Mycobacterium tuberculosis infection of host cells in space and time. *FEMS Microbiology Reviews*, 43, 341–361.

Cardenal-Munoz, E., Barisch, C., Lefrancois, L.H., Lopez-Jimenez, A.T. & Soldati, T. (2017) When Dicty met Myco, a (not so) romantic story about one amoeba and its intracellular pathogen. *Frontiers in Cellular and Infection Microbiology*, 7, 529.

Collinson, L.M., Bosch, C., Bullen, A., Burden, J.J., Carzaniga, R., Cheng, C. et al. (2023) Volume EM: a quiet revolution takes shape. *Nature Methods*, 20, 777–782.

Cornillon, S., Froquet, R. & Cosson, P. (2008) Involvement of Sib proteins in the regulation of cellular adhesion in *Dictyostelium discoideum*. *Eukaryot Cell*, 7, 1600–1605.

Gerstenmaier, L., Pilla, R., Herrmann, L., Herrmann, H., Prado, M., Villafano, G.J. et al. (2015) The autophagic machinery ensures nonlytic transmission of mycobacteria. *Proceedings of the National Academy of Sciences*, 112, E687–E692.

Hagedorn, M., Rohde, K.H., Russell, D.G. & Soldati, T. (2009) Infection by tubercular mycobacteria is spread by nonlytic ejection from their amoeba hosts. *Science*, 323, 1729–1733.

Hagedorn, M. & Soldati, T. (2007) Flotillin and RacH modulate the intracellular immunity of Dictyostelium to Mycobacterium marinum infection. *Cellular Microbiology*, 9, 2716–2733.

Heiligenstein, X., DE Beer, M., Heiligenstein, J., Eyraud, F., Manet, L., Schmitt, F. et al. (2021) HPM live μ for a full CLEM workflow. In: Müller-Reichert, T. & Verkade, P. (Eds.) *Methods in cell biology*. Cambridge, MA: Academic Press.

Humbel, B. & Müller, M. (1985) Freeze substitution and low temperature embedding. *Scanning Electron Microscopy*, 4, 19.

Iwadate, Y. & Yumura, S. (2008) Actin-based propulsive forces and myosin-II-based contractile forces in migrating Dictyostelium cells. *Journal of Cell Science*, 121, 1314–1324.

Kaneko, Y. & Walther, P. (1995) Comparison of ultrastructure of germinating pea leaves prepared by high-pressure freezing-freeze substitution and conventional chemical fixation. *Journal of Electron Microscopy*, 44, 104–109.

Kommnick, C. & Hensel, M. (2021) Correlative light and scanning electron microscopy to study interactions of *Salmonella enterica* with polarized epithelial cell monolayers. *Methods in Molecular Biology*, 2182, 103–115.

Koonce, M., Tikhonenko, I. & Gräf, R. (2020) Dictyostelium cell fixation: two simple tricks. *Methods and Protocols*, 3, 47.

Kreitmeier, M., Gerisch, G., Heizer, C. & Müller-Taubenberger, A. (1995) A Talin homologue of Dictyostelium rapidly assembles at the leading edge of cells in response to chemoattractant. *The Journal of Cell Biology*, 129, 179–188.

Kremer, J.R., Mastronarde, D.N. & Mcintosh, J.R. (1996) Computer visualization of three-dimensional image data using IMOD. *Journal of Structural Biology*, 116, 71–76.

Krentzel, D., Elphick, M., Domart, M.-C., Peddie, C.J., Laine, R.F., Henriques, R. et al. (2023) CLEM-reg: an automated point cloud based registration algorithm for correlative light and volume electron microscopy. *bioRxiv*, 2023.05.11.540445.

Kukulski, W., Schorb, M., Welsch, S., Picco, A., Kaksonen, M. & Briggs, J.A.G. (2011) Correlated fluorescence and 3D electron microscopy with high sensitivity and spatial precision. *The Journal of Cell Biology*, 192, 111–119.

Lee, H.J., Woo, Y., Hahn, T.W., Jung, Y.M. & Jung, Y.J. (2020) Formation and maturation of the phagosome: a key mechanism in innate immunity against intracellular bacterial infection. *Microorganisms*, 8, 1298.

Lerner, T.R., Queval, C.J., Lai, R.P., Russell, M.R., Fearns, A., Greenwood, D.J. et al. (2020) Mycobacterium tuberculosis cords within lymphatic endothelial cells to evade host immunity. *JCI Insight*, 5, e136937.

Lim, J.J., Grinstein, S. & Roth, Z. (2017) Diversity and versatility of phagocytosis: roles in innate immunity, tissue remodeling, and homeostasis. *Frontiers in Cellular and Infection Microbiology*, 7, 191.

Lombardi, M.L., Knecht, D.A. & Lee, J. (2008) Mechano-chemical signaling maintains the rapid movement of Dictyostelium cells. *Experimental Cell Research*, 314, 1850–1859.

López-Jiménez, A.T., Cardenal-Muñoz, E., Leuba, F., Gerstenmaier, L., Barisch, C., Hagedorn, M. et al. (2018) The ESCRT and autophagy machineries cooperate to repair ESX-1-dependent damage at the Mycobacterium-containing vacuole but have opposite impact on containing the infection. *PLoS Pathogens*, 14, e1007501.

Malinovska, L., Palm, S., Gibson, K., Verbavatz, J.-M. & Alberti, S. (2015) Dictyostelium discoideum has a highly Q/N-rich proteome and shows an unusual resilience to protein aggregation. *Proceedings of the National Academy of Sciences*, 112, E2620–E2629.

Mazia, D., Schatten, G. & Sale, W. (1975) Adhesion of cells to surfaces coated with polylysine. Applications to electron microscopy. *The Journal of Cell Biology*, 66, 198–200.

McDonald, K.L. & Auer, M. (2006) High-pressure freezing, cellular tomography, and structural cell biology. *BioTechniques*, 41, 137–143.

Mijanović, L. & Weber, I. (2022) Adhesion of Dictyostelium amoebae to surfaces: a brief history of attachments. *Frontiers in Cell and Development Biology*, 10, 910736.

Moor, H. (1987) Theory and practice of high pressure freezing. In: Steinbrecht, R.A. & Zierold, K. (Eds.) *Cryotechniques in biological electron microscopy*. Berlin, Heidelberg: Springer Berlin Heidelberg.

Pang, K.M., Lee, E., Knecht, D.A. (1998). Use of a fusion protein between GFP and an actin-binding domain to visualize transient filamentous-actin structures. *Current Biology*, 8, 405–408.

Romero-Brey, I. & Bartenschlager, R. (2015) Viral infection at high magnification: 3D electron microscopy methods to analyze the architecture of infected cells. *Viruses*, 7, 6316–6345.

Ronchi, P., Machado, P., D'imprima, E., Mizzon, G., Best, B.T., Cassella, L. et al. (2021) Fluorescence-based 3D targeting of FIB-SEM acquisition of small volumes in large samples. *bioRxiv*, 2021.01.18.427072.

Russell, M.R., Lerner, T.R., Burden, J.J., Nkwe, D.O., Pelchen-Matthews, A., Domart, M.C. et al. (2017) 3D correlative light and electron microscopy of cultured cells using serial blockface scanning electron microscopy. *Journal of Cell Science*, 130, 278–291.

Serra Lleti, J.M., Steyer, A.M., Schieber, N.L., Neumann, B., Tischer, C., Hilsenstein, V. et al. (2022) CLEMSite, a software for automated phenotypic screens using light microscopy and FIB-SEM. *Journal of Cell Biology*, 222, e202209127.

Small, J.V. (1981) Organization of actin in the leading edge of cultured cells: influence of osmium tetroxide and dehydration on the ultrastructure of actin meshworks. *Journal of Cell Biology*, 91, 695–705.

Sosinsky, G.E., Crum, J., Jones, Y.Z., Lanman, J., Smarr, B., Terada, M. et al. (2008) The combination of chemical fixation procedures with high pressure freezing and freeze substitution preserves highly labile tissue ultrastructure for electron tomography applications. *Journal of Structural Biology*, 161, 359–371.

Uchikawa, T., Yamamoto, A. & Inouye, K. (2011) Origin and function of the stalk-cell vacuole in Dictyostelium. *Developmental Biology*, 352, 48–57.

Vanhecke, D., Graber, W. & Studer, D. (2008) Close-to-native ultrastructural preservation by high pressure freezing. In: *Methods in cell biology*. Cambridge, MA: Academic Press.

Verkade, P. (2008) Moving EM: the rapid transfer system as a new tool for correlative light and electron microscopy and high throughput for high-pressure freezing. *Journal of Microscopy*, 230, 317–328.

Villinger, C., Gregorius, H., Kranz, C., Höhn, K., Münzberg, C., Von Wichert, G. et al. (2012) FIB/SEM tomography with TEM-like resolution for 3D imaging of high-pressure frozen cells. *Histochemistry and Cell Biology*, 138, 549–556.

Weber, I., Wallraff, E., Albrecht, R. & Gerisch, G. (1995) Motility and substratum adhesion of Dictyostelium wild-type and cytoskeletal mutant cells: a study by RICM/bright-field double-view image analysis. *Journal of Cell Science*, 108(Pt 4), 1519–1530.

Weiner, A. & Enninga, J. (2019) The pathogen–host Interface in three dimensions: correlative FIB/SEM applications. *Trends in Microbiology*, 27, 426–439.

Weiner, A., Mellouk, N., Lopez-Montero, N., Chang, Y.Y., Souque, C., Schmitt, C. et al. (2016) Macropinosomes are key players in early shigella invasion and vacuolar escape in epithelial cells. *PLoS Pathogens*, 12, e1005602.

Wessels, D., Vawter-Hugart, H., Murray, J. & Soll, D.R. (1994) Three-dimensional dynamics of pseudopod formation and the regulation of turning during the motility cycle of Dictyostelium. *Cell Motility and the Cytoskeleton*, 27, 1–12.

SUPPORTING INFORMATION

Additional supporting information can be found online in the Supporting Information section at the end of this article.

How to cite this article: Franzkoch, R., Anand, A., Breitsprecher, L., Psathaki, O.E. & Barisch, C. (2024) Resolving exit strategies of mycobacteria in *Dictyostelium discoideum* by combining high-pressure freezing with 3D-correlative light and electron microscopy. *Molecular Microbiology*, 121, 593–604. Available from: https://doi.org/10.1111/mmi.15205